J Mater Sci (2009) 44:6563–6570
DOI 10.1007/s10853-009-3629-y

MESOSTRUCTURED MATERIALS

Confined palladium colloids in mesoporous frameworks for carbon nanotube growth

Angel Berenguer-Murcia · Evgeny V. Rebrov · Maciej Cabaj · Andrew E. H. Wheatley · Brian F. G. Johnson · John Robertson · Jaap C. Schouten

Received: 29 November 2008 / Accepted: 19 May 2009 / Published online: 9 June 2009

Abstract Palladium colloidal nanoparticles with an average size of approximately 2.4 nm have been incorporated into mesoporous inorganic thin films following a multistep approach. This involves the deposition of mesoporous titania thin films with a thickness of 200 nm by spin-coating on titanium plates with a superhydrophilic titania outer layer and activation by calcination in a vacuum furnace at 573 K. Nanoparticles have been confined within the porous titania network by dip-coating noble metal suspensions onto these mesoporous thin films. Finally, the resulting nanoconfined systems were used as substrates for the growth of oriented carbon nanotubes (CNTs) using plasma-enhanced chemical vapour deposition at 923 K in order to enhance their surface area. These CNTs were tested in the hydrogenation of phenylacetylene by hydrogen in a batch reactor. The initial reaction rate observed on a CNT/TiO_2 structured catalyst was considerably higher than that on 1 wt% Pd/TiO_2 thin films.

A. Berenguer-Murcia · M. Cabaj · A. E. H. Wheatley · B. F. G. Johnson
Department of Chemistry, University of Cambridge, Lensfield Road, CB2 1EW Cambridge, UK

E. V. Rebrov · J. C. Schouten (✉)
Department of Chemical Engineering and Chemistry, Eindhoven University of Technology, PO Box 513, 5600 MB Eindhoven, The Netherlands
e-mail: j.c.schouten@tue.nl

J. Robertson
Department of Engineering, University of Cambridge, CB2 1PZ Cambridge, UK

Introduction

One of the challenges that must be tackled for the application of efficient catalytic reactors is the development of *high surface area* microsystems. Such devices have, in the first instance, been developed by the etching of 50–300 micron-sized channels on different substrates [1] with a view to performing desired reactions in the absence of heat and mass transfer limitations. The next step towards higher surface area systems that also offered improved substrate accessibility was made by growing layers of microporous zeolites [2] and mesoporous thin films [3] on different substrates. This improvement, however, is not devoid of disadvantages. These arise from the small pore sizes of microporous materials and the relatively small surface areas available in the case of large pore mesoporous materials. In this respect, it should be noted that the growth of tethered carbon nanotubes (CNTs) may represent a promising alternative by which to increase the active surface area. Surface-bound, catalytic chemical vapour deposition (CVD) allows a high degree of structural control and the ability to tailor CNT structure [4]. To achieve this, colloidal precursors are preferred as growth catalysts since they may be prepared with a predefined and narrow size distribution and may be uniformly applied to substrates with uneven geometries [5]. To avoid sintering of the colloidal nanoparticles during heating, they can be dispersed into the mesoporous matrices of thin inorganic films [6].

Multiphase reactions can be performed in structured systems that have a catalytic coating. Usually, however, the geometric surface of these devices needs to be enlarged in order to achieve compelling performance. The efficient use of catalytic reactors requires shaping of the catalyst by deposition of thin catalytic coatings on the walls of the reactor channels or other adequate surfaces. Lately,

inorganic mesoporous thin films have attracted considerable attention because of their large surface areas and narrow pore size distributions, which make them attractive candidates for catalyst supports [7]. Previous studies have shown that colloidal nanoparticles can represent excellent hydrogenation catalysts when they are activated on mesoporous media [8].

The preparation of bimetallic colloids has attracted increasing attention in recent years [8–15]. The presence of a second metal generally improves catalyst properties such as activity, selectivity and/or stability [16]. One of the main aspects of interest in the field of heterogeneous catalysis is the preparation of the catalyst. Nevertheless, despite the large diversity of synthetic methodologies available [17], the precise tuning of size and composition of catalyst particles remains difficult. In this sense, the prior preparation of bimetallic nanoparticles that can be subsequently deposited on a selected support is seen as a suitable alternative to conventional fabrication methods since both composition and particle size can be controlled [18, 19]. Thus, it is possible to prepare bimetallic alloy nanoparticles of perfectly defined composition and structure [18].

The objective of the present study is to deposit nanoparticle-doped mesoporous titania thin films on titanium substrates by spin-coating. Nanoparticle doping of the thin films has been performed by introducing nanoparticles in the thin film by a double coating method which involves spin-coating of a thin mesoporous film followed by dip-coating of the activated thin film in a colloidal nanoparticle suspension. The thin films produced have then been used for the growth of aligned CNT arrays for the production of tailored surfaces with enlarged areas with a view to fabricating structured reactors. Finally, these novel systems have been tested in the hydrogenation of phenylacetylene under mild conditions.

Experimental

Synthesis of Pd-doped mesoporous TiO_2 thin films

Titanium substrates (99.99 + wt% Ti) of 9 × 9 mm^2 and with a thickness of 500 μm were cleaned by immersion in boiling toluene for 1 h to remove organic contaminants from the surface, dried in an oven at 413 K, and weighed. To remove contaminants from the surface oxide layer [20], the titanium substrates were treated with a mixture (180 mL) containing 4.3 vol% H_2O_2 (Fluka) and 3.6 vol% NH_4OH at 353 K for 45 s [21]. The substrates were then rinsed with demi-water and treated with a 4 M NaOH solution at 333 K for 30 s. The plates were rinsed again with demi-water and placed in an oven at 353 K for 30 min. The plates were oxidized at 333 K for 6 h in a 30 vol% aqueous H_2O_2 solution and calcined at 773 K to remove peroxide species. Immediately prior to the synthesis, the titania layer was made super hydrophilic (concentration of surface OH groups >15/nm^2) by UV treatment for 2 h to encourage better adhesion of the titania film to the substrate.

Colloidal palladium nanoparticles with a mean particle diameter of 2.4 nm were synthesized using a well-established approach [22]. These colloids were incorporated in the inorganic matrices of mesoporous thin films as follows: A titania precursor sol of composition 1.0 $Ti(OPr^i)_4$: 0.005 F127: 40 EtOH: 1.3 H_2O: 0.13 HNO_3 was synthesized. The solution was prepared by dissolving the templating agent (Pluronic F127, BASF) in absolute ethanol, followed by the addition of water and nitric acid. Titanium (IV) isopropoxide was added dropwise to the rapidly stirred solution and the resulting mixture was left to age under stirring for 2 h at room temperature.

A sol volume of 50 μL was deposited on activated titanium substrates [1] and the substrates were spin-coated at 1500 rpm for 30 s to spread the solution for full substrate coverage. The spin coater (Laurell) was located in a glove-box at a relative humidity of 80%. The as-synthesized films were kept overnight at the same relative humidity. Drying and calcination were performed in an oven at a residual pressure of 15 mbar. The heating rate from 298 to 573 K was 1 K/min with a 1-h dwelling time every 25 K below 473 K, a 2-h dwelling time at 498, 523, and 548 K, and a 4-h dwelling time at 300 K.

After calcination, the thin films were dip-coated in an ethanol suspension of the Pd nanoparticles with a concentration of 0.06 mg/mL. The resulting samples were left to dry at room temperature and used for the growth of oriented CNTs.

CNT growth

CNTs were grown by plasma-enhanced chemical vapour deposition (PECVD). The coated substrates were loaded into a chamber, which was then evacuated to a residual pressure of 0.6 mbar and heated up to 923 K, with an average heating rate of 40 K/min. An ammonia flow to the sample was then established, providing 0.6 mbar of residual ammonia pressure. The samples were maintained under these conditions for 10 min, then the DC discharge was ignited (600 V, <20 W power), and ammonia was replaced by an ammonia/C_2H_2 mixture (4:1 molar), while the residual pressure was increased to 0.7 mbar. CNT growth was performed for 30 min.

Characterization of the thin films

As-grown samples were characterized using a scanning electron microscope (SEM, Philips XL30 FEGSEM)

operating at 5 kV. The morphology of the coatings was determined by transmission electron microscopy (TEM). High-resolution TEM studies of the scratched films were performed using a JEOL JEM-3011 electron microscope operating at 300 kV with a structural resolution of 0.16 nm. Ellipsometric porosimetry (EP) was used to determine the mean pore size, pore size distribution, and mesopore surface area. Prior to adsorption, the samples were treated under a residual pressure of 0.1 mbar at 573 K for 30 min to remove all adsorbed species. The temperature was then decreased to 287 K and the ethanol (Merck, 99.99 wt%) partial pressure was increased to saturation pressure. The lowest partial pressure of ethanol was 0.10 mbar and the saturation pressure, calculated by Antoine's equation, was 41 mbar. The pore volume and the film thickness were determined from the change in the effective refractive index in the range 300–1200 nm using the Bruggerman Effective Media Approximation (BEMA). The pore size distribution was determined from desorption isotherms using the modified Deriaguin-Broekhoff-de Boer (DBdB) theory with the cylindrical model.

Catalytic activity tests

For each of the catalytic tests, 10 CNT/Pd-TiO_2/Ti plates were fixed in a holder at a 10-mm separation. The holder was placed in an autoclave reactor. In *the first series of tests*, reduction of the CNT/Pd-TiO_2/Ti films was undertaken at 521 K and 10 bar H_2 for 1 h. The reactor was then cooled to 313 K. A 0.008 M solution of phenylacetylene in methanol (130 mL) was deoxygenated by pressurising with H_2 to 5 bar prior to transfer to the reactor. Hydrogenation was performed at 313 K and 10 bar H_2 with the plate holder rotating at 1500 rpm. In *the second series*, the hydrogenation was performed under the same reaction conditions without pre-reduction in hydrogen. *In the third series*, the conditions were the same as for the second series, with the exception that the concentration of substrate was 0.018 M. Analysis was performed by introducing aliquots (2 μL) at established time intervals into a Varian CP-3800 GC equipped with a CP-Sil 5 CB capillary column (diameter: 1 mm, length: 30 m) via an automatic rapid on-line sampler-injector system (ROLSI^{TM}).

Results and discussion

It is fundamentally important to establish that the deposited thin films show the morphology necessary to act as suitable hosts for the confinement of nanoparticles. Figure 1 shows TEM images of these films before and after dip-coating in the suspension of Pd nanoparticles.

As expected, adsorption of the nanoparticles into the pores of the thin film does not significantly alter the mesoporous structure. Figure 1b shows that the nanoparticles (i.e., the dark spots) are present in the mesopores after dip-coating. This observation implies that the nanoparticles are adsorbed on the pore surfaces, although precise determination of their location (i.e., inside the pore or at the pore mouth) will be discussed later. According to the protocol described in the "Experimental" section, the loading of each individual plate should have been 0.37 μg of Pd. In order to corroborate this data, 10 plates were treated with aqua regia and the resulting solution was analyzed by ICP-AES. The observed loading (0.35 μg of Pd per plate) was in close agreement with the expected value. Once adsorbed, the nanoparticles are isolated and can thus perform independently, in the absence of any detrimental effects such as particle agglomeration.

Figure 2 shows the ethanol adsorption–desorption isotherms obtained for a TiO_2 thin film. These data represent typical type IV isotherms and, as such, are characteristic of mesoporous solids. The observation of a type H2 hysteresis loop in the isotherm is normally indicative of there being

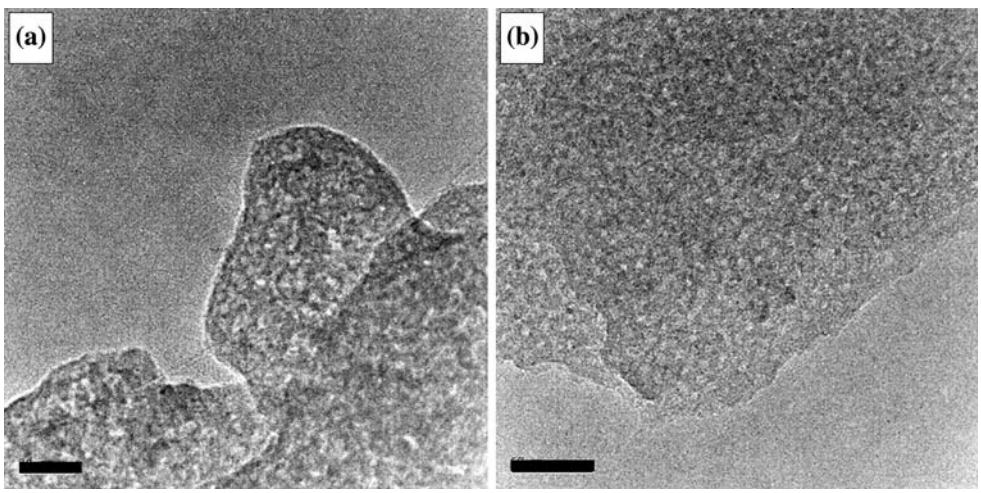

Fig. 1 TEM images of the TiO_2 thin films obtained **a** before and **b** after dip-coating in a Pd nanoparticle suspension. *Scale bars*: **a** 20 nm; **b** 50 nm

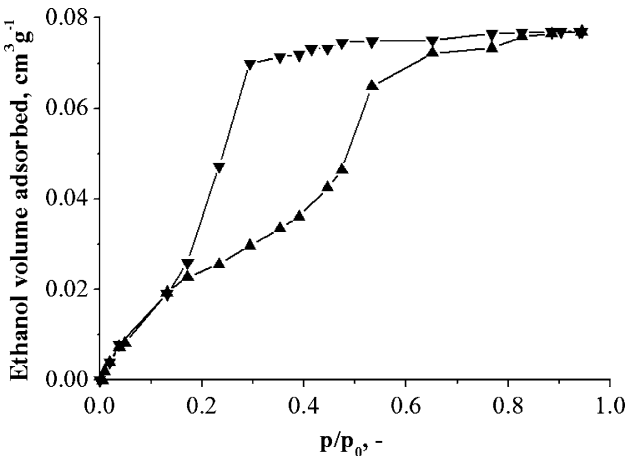

Fig. 2 Ethanol adsorption–desorption isotherms obtained at 287 K for a TiO_2 thin film deposited on a silicon wafer (▲, adsorption branch; ▼, desorption branch)

large pores with small openings. Whilst in the case of a mesoporous material, these features might be associated with a cubic mesoporous network [23], it must be noted that, from Fig. 1b, the developed mesostructure is closer to having a 3D wormhole structure rather than a sharply defined cubic structure [24]. By EP, the titania films have a mean pore opening of 2 nm (after applying the DBdB theory to the isotherm desorption branch), and an open porosity of 17%. However, it must be noted that if the same theory is applied to the adsorption branch the resulting average pore size is 4 nm, which is closer to the value suggested by the TEM images (see Fig. 1b). Thus, considering the colloid size, it seems possible that the particles might be sitting on the outer pore openings, which would imply that they are very close to the surface of the thin film, leaving them readily available for CNT growth. While this result shows that the mesostructure is not completely developed, the sharp ethanol uptake in the adsorption isotherm at a P/P_0 ratio of 0.5 clearly indicates the presence of pores with a narrow size distribution within the mesopore region. Thus, the methodology employed in this study has delivered thin films that show an appropriate 3D network of pores that are suitably sized for hosting the aforementioned nanoparticles.

The SEM images presented in Fig. 3 clearly show excellent coverage of the surface of the thin film, there being no significant surface defects or cracks, after the CNT growth step, with a CNT forest present at the surface of the composite material after PECVD treatment. In comparison to our previous results, obtained using pure Pd nanoparticles to grow CNT forests in the absence of a mesoporous thin film [25–28], the CNTs grown herein show a smaller average diameter (20.6 ± 6.8 nm in [25] versus 10.7 ± 5.7 nm presently). This is a clear indication that the porous network of the titania film is not only able to efficiently adsorb the Pd nanoparticles, but that it also prevents their agglomeration at high temperature during the CNT growth process. It should be noted also that, excluding those obtained using Fe-catalysts, PECVD-grown CNTs do not tend to include nitrogen in their structure, despite the use of ammonia for annealing [28]. It must be noted that despite the fact that CNTs have previously been used as catalyst supports in a variety of reactions [29–32], the present study represents, to the best of our knowledge, the first attempt to fabricate CNTs as an integral part of the reaction system and by which to provide additional surface area. In order to quantify the additional surface provided by the grown CNTs, several areas of 200×200 nm^2 were scanned in order to count both the density of carbon nanotubes and their average length. The average density was of 32 CNTs per area, with an average length of 181 nm. Considering the aforementioned average diameter, the grown CNTs account for an additional 9.2% in external surface area, assuming that the deposited mesoporous TiO_2 coating has a thickness of 170 nm with an apparent density of 1.56 g cm^{-3} [33]. This represents a significant increase in the surface, especially since the area provided by the grown CNTs corresponds to external surface area which is readily available either as a catalyst support or as substrate on which a reaction may be performed.

The activity of catalysts was determined in the hydrogenation of phenylacetylene under mild conditions (313 K, 10 bar H_2). It must be noted that under these reaction

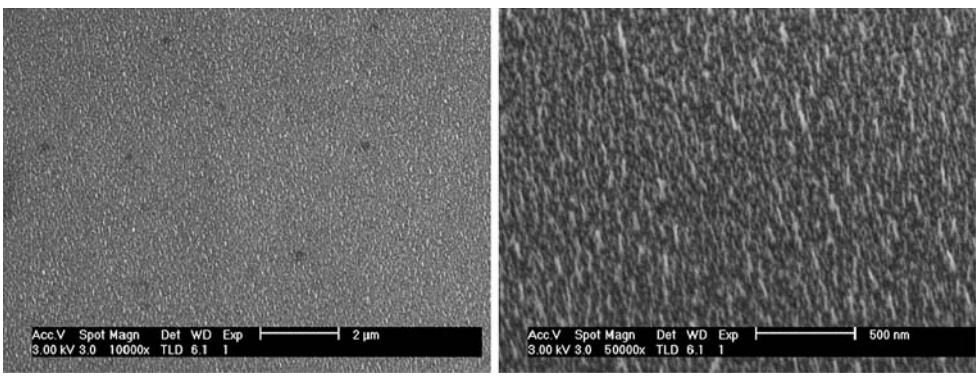

Fig. 3 SEM images of CNT arrays grown using the Pd-doped titania thin films as substrates. *Left*: Upper view of a large area homogeneously covered with CNTs; *Right*: Detailed view of the CNTs

conditions phenylacetylene converts into both styrene and ethylbenzene via two parallel reactions, as could be observed upon monitoring the first minutes of the run, where the formation of ethylbenzene was evident. The mechanism by which this occurs seems to be different from that observed for Pd/TiO_2 thin films, where selectivity towards styrene monotonously decreased during the course of the reaction, confirming a consecutive mechanism of hydrogenation.

For the similar liquid-phase hydrogenation of phenylacetylene over palladium [34] under comparably mild conditions (Scheme 1), it has been reported that mass-transfer effects on the reaction rate are small compared to the overall reaction rate. Therefore, Langmuir–Hinshelwood (LH) kinetics can be applied without including mass-transfer in the modeling (Eqs. 1–3),

$$r_Y = \frac{dC_Y}{dt} = \frac{-(k_1 + k_3)K_Y C_Y C_{H_2}}{1 + K_Y C_Y + K_E C_E + K_A C_A} \quad (1)$$

$$r_E = \frac{dC_E}{dt} = \frac{k_1 K_Y C_Y C_{H_2}}{1 + K_Y C_Y + K_E C_E + K_A C_A} - \frac{k_2 K_E C_E C_{H_2}}{1 + K_Y C_Y + K_E C_E + K_A C_A} \quad (2)$$

$$r_A = \frac{dC_A}{dt} = \frac{k_2 K_E C_E C_{H_2}}{1 + K_Y C_Y + K_E C_E + K_A C_A} + \frac{k_3 K_Y C_Y C_{H_2}}{1 + K_Y C_Y + K_E C_E + K_A C_A} \quad (3)$$

where k_n is the rate constant for reaction n, K_Y, K_E, and K_A are the adsorption constants, and C_Y, C_E, C_A are the concentrations of alkyne, alkene, and alkane, respectively. The hydrogen concentration ($C_{H_2} = 48$ mol/m^3) was calculated from existing solubility data [35]. Figure 4a and b shows the concentration of alkyne, alkene, and alkane as a function of time for series 1 and 2, respectively (results for run 3 not shown). The kinetic parameters are listed in Table 1.

To model the reaction satisfactorily in terms of selectivity as well, it is necessary to add a direct alkyne-to-alkane hydrogenation step. In practice such a one-step

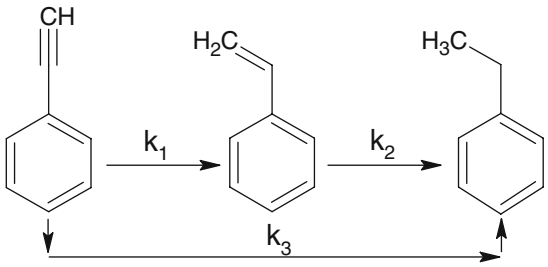

Scheme 1 Hydrogenation of phenylacetylene

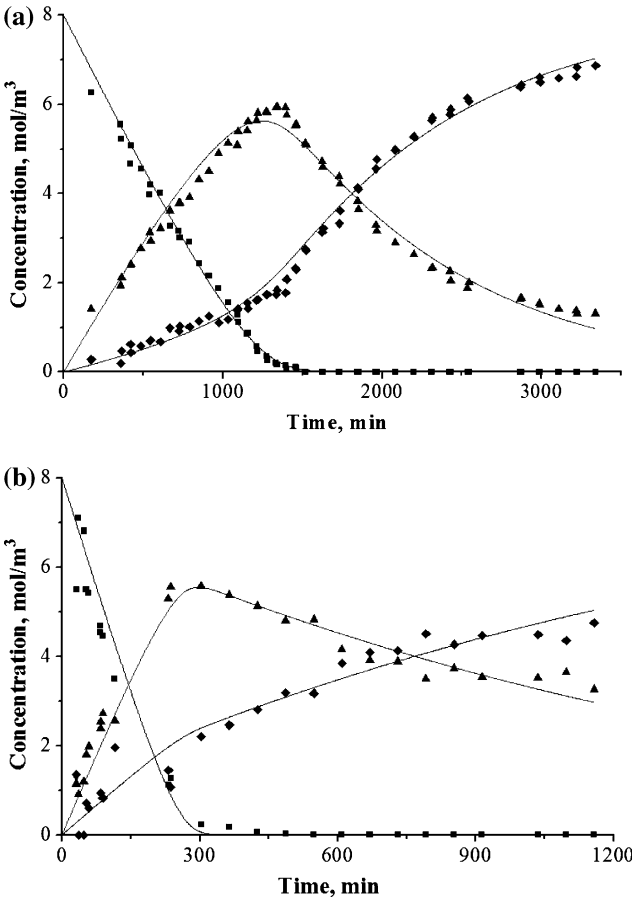

Fig. 4 LH kinetics model versus experimental data. Hydrogenation of phenylacetylene on CNF/TiO_2/Ti coatings (10 substrate plates 1 × 1 cm^2, initial alkyne concentration: 8.0 mol/m^3). *Markers*: experiment, (■) alkyne concentration, (▲) alkene concentration, (◆) alkane concentration. *Lines*: kinetic fit. **a** Series 1. **b** Series 2. Series 3 is not shown. First 120 min of experiment are not included in fitting. Reaction conditions: $T = 313$ K, $P_{H_2} = 10$ bar

hydrogenation is unlikely. Instead, it is more likely that the alkene produced on the catalyst surface is hydrogenated further to the alkane, before it has a chance to desorb, i.e., the catalyst surface composition is not in equilibrium with the surrounding liquid, which is not taken into account in the present model. It should be noted that the kinetic parameters obtained in the second and third series are the same, while being markedly different from run 1.

A 99.9% conversion of alkyne was reached after 1440 and 300 min, respectively, in the first and second series. This is because the rate constants k_1 and k_3 increased by 3.9 and 9.6 times, respectively, in the second series, while the rate constant k_2 remains relatively unchanged. It can be seen that both alkene and alkane have been produced from the beginning of the reaction. However, the ratio of adsorption constants of alkyne and alkene (K_Y/K_E) is above 35, so the strong alkyne adsorption should prevent adsorption of alkene on the surface. Therefore, it appears that there exists another parallel route for the hydrogenation of alkyne. This

Table 1 Parameter values for the LH model in the hydrogenation of phenylacetylene on CNF/TiO_2/Ti coatings at 313 K

Run	k_1, min^{-1}	k_2, min^{-1}	k_3, min^{-1}	K_Y, m^3 mol^{-1}	K_E, m^3 mol^{-1}	K_A, m^3 mol^{-1}
1	1.35×10^{-4}	3.44×10^{-4}	2.03×10^{-5}	2.54	7.03×10^{-2}	1.25×10^{-2}
2	5.27×10^{-4}	2.95×10^{-4}	1.95×10^{-4}	2.54	7.03×10^{-2}	1.25×10^{-2}
3	5.27×10^{-4}	2.95×10^{-4}	1.95×10^{-4}	2.54	7.03×10^{-2}	1.25×10^{-2}

can be concluded from the constant initial selectivity, towards alkene, of 86 and 73%, respectively, for series 1 and 2. It must be noted that the results obtained for the TiO_2 thin films loaded with Pd (without performing any CNT growth) were identical to those obtained with their CNT counterparts, although slightly higher selectivities were achieved (e.g., 90% in the case of series 1). The results are in accordance with the ratio of kinetic constants of the two parallel reactions:

$$S_E = \frac{k_1}{k_1 + k_3} \tag{4}$$

In the first series, the hydrogenation of the alkene becomes significant once all the alkyne has been converted, as the k_2/k_3 ratio is 15. However, in the second series this ratio becomes 1.5, meaning that parallel and consecutive mechanisms contribute almost equally to the formation of alkane.

According to the results obtained the parameters fitted after the three reaction runs, the performance of the catalyst is identical in runs 2 and 3, whilst being markedly different to that in run 1. A possible explanation for this behaviour could be reconstruction of the catalytic species with a more dense structure (e.g., by the formation of CNT bundles), resulting in a system which can, on the one hand convert phenylacetylene more efficiently, but on the other hand hinders diffusion of the semi-hydrogenated product away from the catalyst, thus resulting in a greater likelihood of further reaction to give the fully hydrogenated product and decreasing the selectivity towards styrene.

The large contribution of alkane formation via direct hydrogenation of alkyne makes this catalytic system rather different from those in the literature (see, for example, [22] and references therein). This phenomenon may be explained by the state in which the hydrogenation catalyst is present in our case. The Pd nanoparticles that are used in this study are encapsulated within the tips of the grown CNT structures (Fig. 5), with the graphitic layers of the grown CNT representing a potential impediment to diffusive access of the substrate to the Pd surface.

It is well-known that gaseous H_2 can diffuse through the graphitic layers of CNTs, which is the reason why these materials are currently under intensive study for the development of hydrogen storage systems [36]. The fact that the reaction proceeds with the encapsulated Pd nanoparticles seems to indicate that they may be accessed by hydrogen molecules, giving rise to highly active atomic hydrogen upon dissociation at the Pd surface. This would account for the recorded hydrogenation activity. Palladium is an excellent catalyst in semi-hydrogenation reactions due to the marked difference in enthalpies of adsorption between triple and double bonds, the latter enthalpy being much smaller than the former. Thus, phenylacetylene is adsorbed on a Pd surface, hydrogenated to styrene and immediately displaced from the adsorption site by another phenylacetylene molecule. As the reaction proceeds, phenylacetylene is removed from the system, and only when its concentration reaches very low values does styrene begin to undergo hydrogenation. In the present case, however, having rendered the Pd nanoparticles inaccessible, this beneficial effect of the Pd surface is removed, and although the hydrogenation rates for both phenylacetylene and styrene are similar to those reported in the literature, the selectivity values are slightly lower due to the absence of a clean Pd surface on which the substrate may be adsorbed. Thus, the catalytic tip-growth of CNTs under the influence of Pd nanoparticles has clearly achieved the primary aim of enhancing the surface area of the porous coating. While the observed catalytic behaviour points to the ability of the reducing agent to diffuse through the nanotube structure, our data suggest that the use of a second catalyst (e.g., adsorbed/grafted on the CNT surface) may be required if high selectivities (>95%) are desired. Nevertheless, the reported preparation of thin films with enhanced surface area represents a promising prospect for microreactor and/or coating technology since the observed CNT forests offer an increased surface for structured systems, thereby suggesting a route by which to circumvent heat and mass transfer limitations.

Conclusions

We have shown that the use of a mesoporous thin film for the seclusion of noble metal nanoparticles by straightforward dip-coating techniques represents an efficient way to incorporate colloids within a mesoporous titania network following a simple synthetic protocol. Moreover, subsequent CNT synthesis by PECVD has shown that it is possible to catalyze the growth of narrow CNT arrays on the nanoparticle-doped thin films in order to massively increase the available surface area of the microreactor. Catalytic tests show that the system is active in the

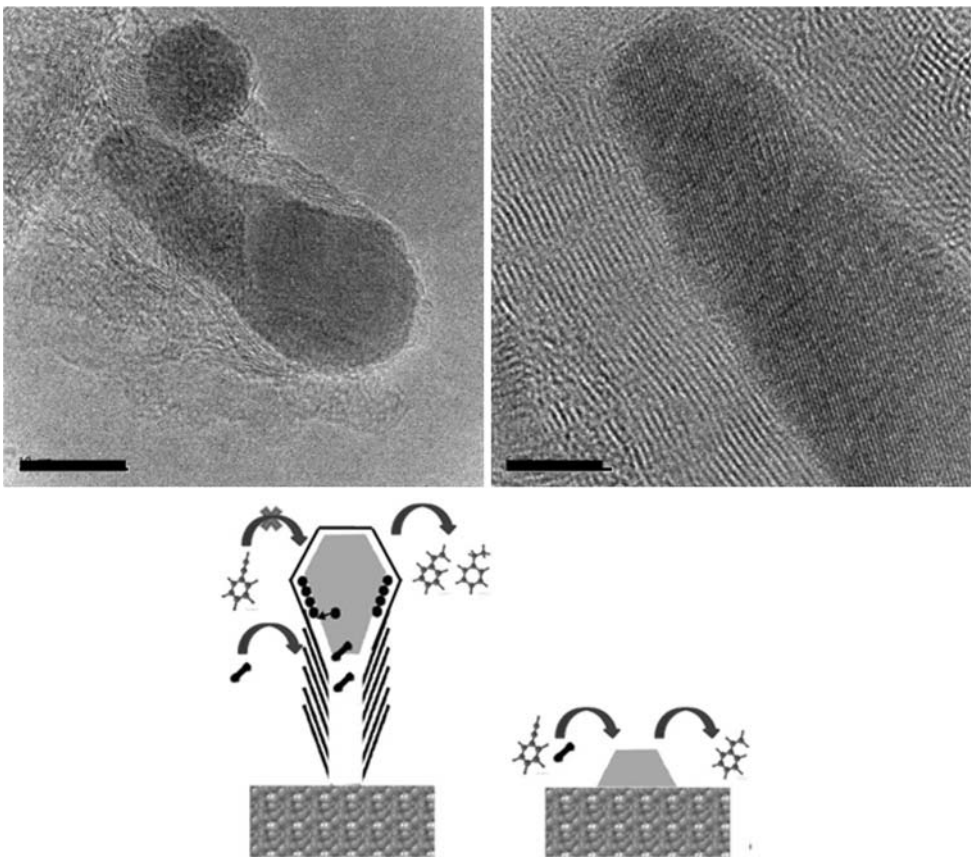

Fig. 5 TEM images of the CNTs grown using PECVD. *Top left*: Tip of a CNT. *Top right*: High-resolution image showing the crystal lattice of the Pd nanoparticle and the graphitic walls. Scale bars: *Left*: 10 nm; *Right*: 5 nm. *Bottom*: Scheme illustrating the diffusional hindrance of phenylacetylene into the CNT structure in comparison with a "naked" nanoparticle

semi-hydrogenation of phenylacetylene, but that whilst dihydrogen is capable of accessing the nanoparticles, their encapsulation by the growing tips of the CNTs restricts access by the organic substrate. The result is that whilst hydrogenation activity is recorded, selective formation of the alkene is slightly lower than that reported for other systems due to the lack of preferential adsorption sites for the selective hydrogenation of triple bonds to double bonds. The synthesized systems can thus be regarded as structured surfaces with greatly enlarged area that promise applications as supports for state-of-the-art microreactors. These promise to remove present heat and mass transfer restrictions through subsequent nanoparticle fabrication of the grown CNTs.

Acknowledgements The authors would like to acknowledge the European Commission (*NOE* EXCELL NMP3-CT-2005-515703), the British Research Council, and Netherlands Organisation for Scientific Research (NWO) (Projects PPS-888 and PPS-894) for financial support. The authors would also like to acknowledge MSc. Lidia Protasova for her kind help with the ethanol adsorption isotherms analysis.

References

1. Hessel V, Hardt S, Löwe H (2004) Chemical micro process engineering: fundamentals, modelling and reactions. Wiley, New York
2. Mies MJM, Rebrov EV, Jansen JC et al (2007) Micropor Mesopor Mater 106(1–3):95
3. Muraza O, Rebrov EV, Khimyak T et al (2008) Chem Eng J 135(Suppl 1):S99
4. Dai HJ (2002) Acc Chem Res 35:1035
5. Golovko VB, Li HW, Kleinsorge B et al (2005) Nanotechnology 16:1636
6. Kind H, Bonard J-M, Forro L et al (2000) Langmuir 16:6877
7. Glazneva TS, Rebrov EV, Schouten JC et al (2007) Thin Solid Films 515:6391
8. Sinfelt JH (1983) Bimetallic catalysts, an Exxon monograph. Wiley, New York
9. Kuroda H, Iwasawa Y (1989) Intl Rev Phys Chem 8:207
10. Johnson BFG (2003) Topics Catal 24(1–4):147
11. Raja R, Golovko VB, Thomas JM et al (2005) Chem Comm 15:2026
12. Baughman RH, Zakhidov AA, de Heer WA (2002) Science 297:787
13. Choi YS, Cho YS, Kang JH et al (2003) Appl Phys Lett 82:3565
14. Niu C, Sichel EK, Hoch R et al (1997) Appl Phys Lett 70:1480
15. Kleinsorge B, Golovko VB, Hofmann S et al (2004) Chem Comm 1416
16. Román-Martínez MC, Cazorla-Amorós D, de Miguel S et al (2004) J Jpn Petrol Inst 47(3):164
17. Haber J, Block JH, Delmon B (1995) Pure Appl Chem 67:1257

18. Wunder RW, Philips J (1996) J Phys Chem 100:14430
19. Bönnemann H, Richards RM (2001) Eur J Inorg Chem 10:2455
20. Teixeira RLP, de Godoy GCD, Pereira MM (2004) Mater Res 7:299 (online)
21. Mies MJM, Rebrov EV, Jansen JC et al (2007) J Catal 247:328
22. Dominguez-Dominguez S, Berenguer-Murcia A, Cazorla-Amoros A et al (2006) J Catal 243:74
23. Wang K, Morris MA, Holmes JD (2005) Chem Mater 17:1269
24. Grosso D, Soler-Illia GJAA, Crepaldi EL et al (2003) Chem Mater 15:4562
25. Berenguer-Murcia A, Cantoro M, Golovko VB et al (submitted) Phys Stat Solidi
26. Ago H, Murata K, Yumuram M et al (2003) App Phys Lett 82:811
27. Guo T, Nikolaev P, Thess A et al (1995) Chem Phys Lett 243:49
28. Hofmann S, Blume R, Wirth CT et al (2009) J Phys Chem C 113:1648
29. Garcia J, Gomes HT, Serp P et al (2006) Carbon 44(12):2384
30. Serp P, Corrias M, Kalck P (2003) Appl Catal A 253(2):337
31. Vu H, Goncalves F, Philippe R et al (2006) J Catal 240(1):18
32. Dominguez-Dominguez S, Berenguer-Murcia A, Cazorla-Amoros A et al (2008) J Phys Chem C 112(10):3827
33. Rebrov EV, Berenguer-Murcia A, Johnson BFG et al (2008) Catal Today 138(3):210
34. Chaudhari RV, Jaganathan R, Kolhe DS et al (1986) Chem Eng Sci 41:3073
35. Descamps C, Coquelet C, Bouallou C et al (2005) Thermochim Acta 430:1
36. Jordá-Beneyto M, Suárez-García F, Lozano-Castelló D et al (2008) Carbon 45(2):293